Magneto-mechanical resonance of a single superparamagnetic microbead trapped by a magnetic domain wall

Elizabeth Rapoport and Geoffrey S. D. Beach[a)]
Department of Materials Science and Engineering, Massachusetts Institute of Technology, Cambridge, Massachusetts, 02139, USA

(Presented 3 November 2011; received 23 September 2011; accepted 26 October 2011; published online 23 February 2012)

Magnetic domain walls in ferromagnetic tracks can be used to trap and transport superparamagnetic beads for lab-on-a-chip applications. Here it is shown that the magnetostatic binding between a domain wall and a superparamagnetic bead suspended in a host fluid leads to a distinct magneto-mechanical resonance under application of a sinusoidal driving field. The characteristic resonant frequency depends on the ratio of the magnetostatic binding force to the viscous drag on the bead. This resonance has been experimentally detected for a single trapped superparamagnetic bead using an optical detection technique. © *2012 American Institute of Physics*. [doi:10.1063/1.3672406]

Surface-functionalized superparamagnetic (SPM) beads are widely used to tag, detect, and manipulate chemical and biological species in a fluid environment.[1–17] Recent work has shown that, owing to their highly localized stray fields, magnetic domain walls (DWs) in magnetic nanotracks can be used to shuttle superparamagnetic microbeads and magnetically tagged entities across the surface of a substrate.[9–14] By integrating a single-bead detection mechanism into such DW-based transport structures, microscale sorting and sensing of single cells or biomolecules could be achieved in magnetic lab-on-chip devices.

Magnetoresistive sensors have previously been widely used for SPM bead sensing, based on a change in the sensor response to an applied excitation field in the presence of beads at the sensor surface.[1,2,5,7,9,15–17] On-chip bead-based sensing of biomolecules in such devices is often achieved by chemically functionalizing the sensor surface to preferentially capture and immobilize magnetic marker beads in the presence of a chemical target in the host fluid. However, this mode of sensing requires chemical decoration of the sensor surfaces and precludes the subsequent transport of a bead after a sensing operation. Donolato *et al.*[17] have recently demonstrated the detection of magnetic beads suspended in a fluid in close proximity to a magnetic tunnel junction sensor based on Brownian relaxation of the beads themselves. Their technique offers a probe of the hydrodynamic characteristics of the sensed beads, which would change, e.g., if the bead surface were decorated with a chemical target. Biosensing could thus be achieved without the need to chemically tether the bead directly to the sensor. However, sensitivity at the level of single bead sensing has not yet been demonstrated using such a mechanism.

Domain walls in nanotracks can be used to capture individual beads, and DW-based structures have recently been used to sense the presence of individual beads. Llandro *et al.*[7] showed detection of individual beads from the effect of their stray field on DW-mediated magnetization switching in pseudo-spin-valves. Vavassori *et al.*[9] exploited the magnetic focusing of DWs to position a bead near a DW trapped at a nanotrack corner, and to detect the bead's presence based on a small change in the DW depinning field. However, both of these mechanisms rely on sensing small changes to the switching field, which itself is typically stochastic in nature.

Here we show that the bead-DW interaction can be used not only to reversibly trap individual beads for transport, but also to characterize the trapped beads based on their hydrodynamic response within a host fluid. By measuring the response of a trapped bead to a sinusoidally driven domain wall, we show that a characteristic resonant frequency exists that is a function of the bead size and the strength of its interaction with the DW. This magneto-mechanical resonance offers a means to distinguish beads based on their physical characteristics, and could, hence, be exploited to allow DW-based devices to trap, sense, transport, and release individual magnetic beads in one integrated system.

We have modeled the magnetostatic interaction between a DW and a SPM bead using micromagnetics for DW spin structure calculations, and numerical integration to compute the resulting stray field profile and its effect on a model SPM bead. Our approach permits an accurate accounting of both the local field configuration from more complex DW structures (e.g., vortex DWs), and of the superparamagnetism of beads of an experimentally relevant size.

Calculations were performed using the public micromagnetics package OOMMF[18] to compute the relaxed DW structure in a nanotrack. We used the materials parameters for bulk $Ni_{80}Fe_{20}$ (exchange constant $A = 1.3 \times 10^{-11}$ J m^{-1}, saturation magnetization $M_s = 800$ kA m^{-1}, uniaxial anisotropy $K_u = 0$), and a cell size of $5 \times 5 \times 40$ nm^3. The computed DW structure was then used to numerically calculate the DW stray field profile via the scalar potential. Finally, the magnetostatic energy of a spherical SPM bead was calculated as a function of its lateral position in the vicinity of the DW, with demagnetizing effects approximated via a spherical demagnetizing

a)Author to whom correspondence should be addressed. Electronic mail: gbeach@mit.edu.

factor of 1/3. We used a bead volume susceptibility $\chi = 800$ kA m^{-1} T^{-1} corresponding to commercial microbeads,[6] similar to those used in the experiment below.

An example potential energy surface for a 2 μm diameter bead due to the stray field of a vortex DW in a 400 nm wide, 40 nm thick $Ni_{80}Fe_{20}$ track is shown in Fig. 1(a). The potential landscape for these dimensions is nearly parabolic. Thus, for small relative displacements, the bead is tethered to the DW by a linear restoring force arising from the nearly harmonic magnetostatic interaction potential (Fig. 1(b)). As a result of viscous damping in the fluid, the coupled system should exhibit an overdamped resonant response to an external periodic excitation, with a characteristic resonant frequency dependent on the restoring force, F_{int}, and the viscous drag, F_{drag}.

To describe this dynamical response, we assume strongly overdamped conditions and neglect inertial terms to derive an equation of motion for the bead, assuming that the DW position oscillates sinusoidally about a given position. Hence, we assume that the relation,

$$b\frac{dx(t)}{dt} = k(x_{DW}(t) - x(t)), \tag{1}$$

holds, where the left hand term is the Stokes drag on the bead with composite drag coefficient b, and the right hand term is the interaction force, with k the restoring force constant coming from the gradient of magnetostatic potential. Here, the DW and bead positions in time, $x_{DW}(t)$ and $x(t)$, respectively, oscillate sinusoidally at angular frequency ω, with complex amplitudes X_0 and δ, respectively. Solving Eq. (1) for δ yields:

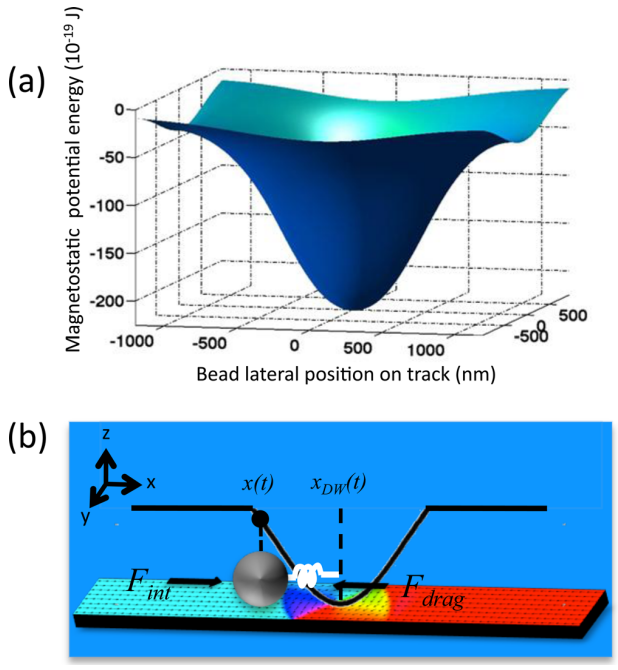

FIG. 1. (Color online) (a) Magnetostatic potential energy vs lateral position for a 2 μm diameter SPM bead at the surface of a 400 nm wide × 40 nm thick $Ni_{80}Fe_{20}$ track containing a vortex wall. (b) Micromagnetically computed domain wall structure in a 400 nm wide × 40 nm thick $Ni_{80}Fe_{20}$ track with a schematic of the oscillator geometry in the bead-DW system.

$$\delta = \frac{\omega_0 X_0}{\omega_0 - i\omega}, \tag{2}$$

where $\omega_0 = k/b$ is the resonant frequency. We can separate the imaginary and real components of δ to obtain the in-phase, δ_1, and out of phase, δ_2, components of bead oscillation:

$$\delta_1 = \mathrm{Re}(\delta) = \frac{X_0}{1 + \left(\frac{\omega}{\omega_0}\right)^2}, \tag{3}$$

$$\delta_2 = \mathrm{Im}(\delta) = \frac{X_0 \frac{\omega}{\omega_0}}{1 + \left(\frac{\omega}{\omega_0}\right)^2}. \tag{4}$$

Thus, from the resonance curve we expect a resonant frequency that is a function of the interaction force and bead size.

We have experimentally characterized the small-amplitude magneto-mechanical resonant response of a trapped bead under sinusoidal drive using the technique outlined in Fig. 2. Arrays of 800 nm wide, 40 nm thick, 30 μm outer diameter $Ni_{80}Fe_{20}$ ring tracks were fabricated on a Si(100) wafer by electron beam lithography, dc-sputter deposition, and subsequent lift off. After lift-off, the entire wafer was covered by a 70 nm thick rf-sputtered SiO_2 protective overcoat.

The ring geometry permits a high degree of control over DW nucleation and positioning. Application of a strong in-plane magnetic field generates two circumferential domains separated by DWs lying along the field axis. These DWs can then be sinusoidally driven around a fixed position by application of a large dc bias field in conjunction with a small amplitude ac field transverse to the pinning dc field (as shown in Fig. 2(a)). In this configuration there is significant transverse field; however, our calculations showed that application of a transverse in-plane field does not appreciably affect the interaction force between a bead and a DW.

During the experiment we first initialized the tracks into the bi-domain state. Then a dilute suspension of SPM microbeads (Dynal Dynabeads Carboxylic Acid from Dynal Biotech, suspended in phosphate buffered saline (PBS) with 0.1% (v/v) Tween 20 detergent, at a concentration of 3×10^5 beads/mL) was placed on the wafer surface. Experiments were performed with bead diameters of either 1.0 μm or 2.8 μm. Bead capture by DW fringing fields was monitored via a CCD camera fitted to a custom microscope apparatus.

Once a bead had been captured by a DW fixed in an equilibrium position by the dc field, an orthogonal ac field, H_{ac}, was used to drive DW oscillations about that position. A laser probe was used to monitor bead motion. The laser probe apparatus used a 532 nm solid-state laser, linearly polarized and attenuated to ~0.1 mW. The laser was focused and collected through a single long working distance microscope objective (N = 0.28). During measurement, the laser was defocused and offset tangentially along the track such that bead oscillation was restricted to one side of the Gaussian profile. The reflected intensity varied monotonically with bead position. At low drive frequencies, bead motion followed the drive field, with reflected intensity dropping (increasing) as the bead

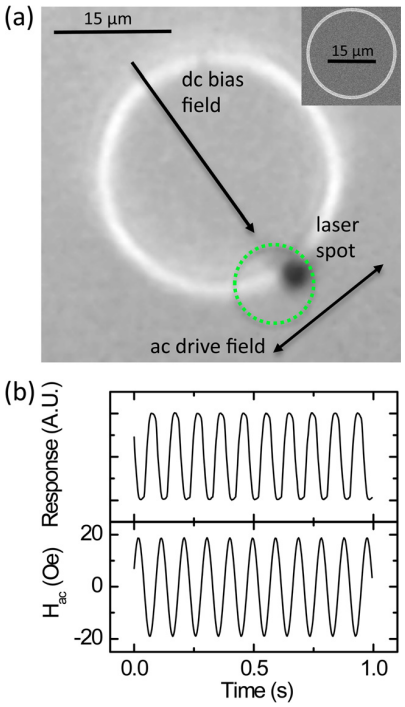

FIG. 2. (Color online) (a) Optical image of a 2.8 μm diameter bead on a 30 μm outer diameter, 800 nm wide, 40 nm thick $Ni_{80}Fe_{20}$ ring (SEM inset), with field configuration and probe laser spot location (green circle). (b) Real time response of reflected laser intensity (top) as a bead is driven in and out of the beam spot by a DW driven by small amplitude, sinusoidal ac field (bottom).

moved into (out of) the beam path. This is shown in Fig. 2(b) for a 2.8 μm bead being driven at 10.5 Hz.

To measure the bead's magneto-mechanical resonance, the reflected intensity response was measured versus drive frequency using a lock-in amplifier. Figure 3 shows the in- and out-of-phase response for $H_{dc} = 250$ Oe and $H_{ac} = 20$ Oe (quasistatic displacement amplitude $\sim$1 μm), for beads of two different diameters. The data are well fitted by the over-damped resonance model described above with resonant frequency 23.5 Hz for the 2.8 μm bead, and 57.0 Hz for the 1.0 μm bead. The significant upward shift in the resonance frequency for the smaller bead is as expected due to the proportionally smaller hydrodynamic drag on the bead.

Magnetic domain walls act as mobile traps for beads, opening up new possibilities for high-throughput sorting and transport with single-bead precision. Here we have shown that the magnetostatic binding between a DW and a trapped bead can be further used to interrogate that bead dynamically, offering a new mechanism for microbead metrology with single-bead sensitivity. Although here we have detected the resonant response of the coupled system optically, this same mechanism could be exploited with electrical sensing using a spin-valve structure for position-sensitive tracking of the DW oscillation. Hence, DWs could be used to reversibly trap and sense not only the presence, but also the physical characteristics, of individual SPM beads in lab-on-chip applications.

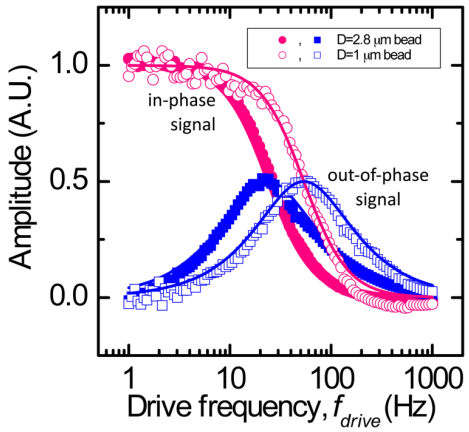

FIG. 3. (Color online) Resonant excitation of trapped 1 μm diameter and 2.8 μm diameter SPM bead in aqueous environment by oscillating DW in circular magnetic track. Curves show in-phase and out-of-phase optical reflectivity signal, approximately proportional to bead oscillation amplitude.

This work was supported in part by the Materials Research Science and Engineering Center Program of the National Science Foundation under award number DMR 0819762 and by the MIT Deshpande Center for Technological Innovation. Device fabrication was carried out at the MIT Nanostructures Laboratory.

[1]D. R. Baselt, G. U. Lee, M. Natesan, S. W. Metzger, P. E. Sheehan, and R. J. Colton, Biosens. Bioelectron. **13**, 731 (1998).
[2]R. L. Edelstein, C. R. Tamanaha, P. E. Sheehan, M. M. Miller, D. R. Baselt, L. J. Whitman, and R. J. Colton, Biosens. Bioelectron. **14**, 805 (2000).
[3]Q. A. Pankhurst, J. Connolly, S. K. Jones, and J. Dobson, J. Phys. D: Appl. Phys. **36**, R167 (2003).
[4]M. A. M. Gijs, Microfluid. Nanofluid. **1**, 22 (2004).
[5]S. X. Wang, S.-Y. Bae, G. Li, S. Sun, R. L. White, J. T. Kemp, and C. D. Webb, J. Magn. Magn. Mater. **293**, 731 (2005).
[6]R. J. S. Derks, A. Dietzel, R. Wimberger-Friedl, and M. W. J. Prins, Microfluid. Nanofluid. **3**, 141 (2007).
[7]J. Llandro, T. Hayward, D. Morecroft, J. A. C. Bland, F. Castaño, I. Colin, and C. Ross, Appl. Phys. Lett. **91**, 203904 (2007).
[8]J. Dobson, Nat. Nanotechnol. **3**, 139 (2008).
[9]P. Vavassori, V. Metlushko, B. Ilic, M. Gobbi, M. Donolato, M. Cantoni, and R. Bertacco, Appl. Phys. Lett. **93**, 203502 (2008).
[10]G. Vieira, T. Henighan, A. Chen, A. Hauser, F. Yang, J. Chalmers, and R. Sooryakumar, Phys. Rev. Lett. **103**, 128101 (2009).
[11]M. Donolato, P. Vavassori, M. Gobbi, M. Deryabina, M. Hansen, V. Metlushko, B. Ilic, M. Cantoni, D. Petti, S. Brivio, and R. Bertacco, Adv. Mater. **22**, 2706 (2010).
[12]T. Henighan, A. Chen, G. Vieira, A. Hauser, F. Yang, J. Chalmers, and R. Sooryakumar, Biophys. J. **98**, 412 (2010).
[13]G. Ruan, G. Vieira, T. Henighan, A. Chen, D. Thakur, R. Sooryakumar, and J. Winter, Nano Lett. **10**, 2220 (2010).
[14]M. Bryan, J. Dean, T. Schrefl, F. Thompson, J. Haycock, and D. Allwood, Appl. Phys. Lett. **96**, 192503 (2010).
[15]R. S. Gaster, L. Xu, S.-J. Han, R. J. Wilson, D. A. Hall, S. J. Osterfeld, H. Yu, and S. X. Wang, Nat. Nanotechnol. **6**, 314 (2011).
[16]B. T. Dalslet, C. D. Damsgaard, M. Donolato, M. Stromme, M. Stromberg, P. Svedlindh, and M. F. Hansen, Lab Chip **11**, 296 (2011).
[17]M. Donolato, E. Sogne, B. T. Dalslet, M. Cantoni, D. Petti, J. Cao, F. Cardoso, S. Cardoso, P. P. Freitas, M. F. Hansen, and R. Bertacco, Appl. Phys. Lett. **98**, 073702 (2011).
[18]M. J. Donahue and D. G. Porter, OOMMF User's Guide Version 1.0, (NIST, Gaithersburg, MD,1999)